Progress in Nuclear Energy 140 (2021) 103920

Contents lists available at ScienceDirect

Progress in Nuclear Energy

journal homepage: www.elsevier.com/locate/pnucene

Increasing productivity in the manufacture of UAl_2–Al dispersion-plate targets for Mo-99 production

Michelangelo Durazzo *, Giovanni L.C.R. Conturbia, Elita F. Urano de Carvalho

Nuclear and Energy Research Institute, IPEN-CNEN/SP, Sao Paulo, Brazil

ARTICLE INFO

Keywords:
Target plates
Irradiation targets
Molybdenum-99
UAl_x-Al
Picture-frame technique
Multiple targets
Fabrication

ABSTRACT

Molybdenum-99 is the most important isotope because its daughter isotope, technetium-99 m, has been the most widely used medical radioisotope. The primary method employed to produce Mo-99 derives from the fission of U-235 incorporated in so-called irradiation targets. Pushed by the international Mo-99 crisis that occurred in 2009/2010, Brazil has decided to construct a new research reactor, the Brazilian Multipurpose Reactor (RMB), to produce this vital radioisotope to meet the Brazilian domestic demand. As part of this effort, it has been developed the process for manufacturing the target to be used in the production of Mo-99 by nuclear fission. The low enriched uranium (LEU) aluminide with the predominant phase UAl_2 was the starting material. The picture-frame technique was used to clad UAl_2–Al briquette with aluminum to obtain plate-type targets. It was developed an innovative method that allows increasing the productivity of this type of target based on multi-core rolling. A thermomechanical treatment was designed to get targets composed basically of a mixture of UAl_3/UAl_4 that are the required phases for a proper radiochemical dissolution after irradiation. The manufacturing process proved to be suitable for domestic production of targets, fulfilling the specification to produce Mo-99 in the Brazilian Multipurpose Reactor.

1. Introduction

According to the Nuclear Energy Agency (2019) information, the world annually demands more than 30 million medical imaging procedures that use the technetium-99m radioisotope (Tc-99m), which corresponds to approximately 80 % of all nuclear medicine diagnoses. Barnowski (2011) reported that technetium-99m is used in over 70 medical procedures, mainly for diagnosing heart disease, tracking the spread of cancer, diagnosing brain diseases, and more applications are developed for its use each year. Tc-99m is derived from the radioactive decay of molybdenum-99 (Mo-99). Because of its short half-life (6 h), the Tc-99m needs to reach the final consumer in the form of Mo-99, as lyophilized kits. The most important method for producing Mo-99 on an industrial scale is fissioning U-235 through neutron irradiation of targets containing uranium in research reactors (Verbeek, 2008).

Currently, Brazil has four research reactors in operation; the more significant is the pool type IEA-R1 running at 5 MW. The others are IPR-R1 (100 kW TRIGA type), ARGONAUTA (500 W Argonaut type), and IPEN/MB-01 (100 W critical facility). As can be noticed, IEA-R1 is the most powerful research reactor in Brazil; even then, it is not powerful enough to produce Mo-99. As a result, all Mo-99 has been imported to meet the domestic demand for nuclear medicine.

Over the last decade, reliable supplying of Mo-99 has been seriously compromised because of unexpected shutdowns and extended refurbishment periods at some research reactors. These factors have led to global shortages of Mo-99, as experienced between 2009 and 2010 and lately in 2017–2018 (Nuclear Energy Agency, 2019).

Brazilian nuclear medicine has also been affected by these global shortages. In 2010, the Brazilian government decided to build a new research reactor to tackle this issue, mainly for domestic Mo-99 production (Obadia and Perrotta, 2010). The new reactor will be a 30 MW open pool-type reactor, using low enriched uranium (LEU) fuel. Perrotta and Soares (2014) describe the key characteristics of the new research reactor, which was named the Brazilian Multipurpose Reactor (RMB). The facility will be part of a new nuclear research center to be built about 100 km from São Paulo city in the southeast part of Brazil. Perrotta and Obadia (2011) provide information about the new research center, which will have several facilities. The targets needed to produce Mo-99 at the RMB research reactor are planned to be produced in Brazil.

Targets used to produce Mo-99 from U-235 fission can be

* Corresponding author. Av. Prof. Lineu Prestes, 2242, University City, 05508-000, Sao Paulo, SP, Brazil.
E-mail address: mdurazzo@ipen.br (M. Durazzo).

https://doi.org/10.1016/j.pnucene.2021.103920
Received 25 April 2021; Received in revised form 19 June 2021; Accepted 2 August 2021
Available online 6 August 2021

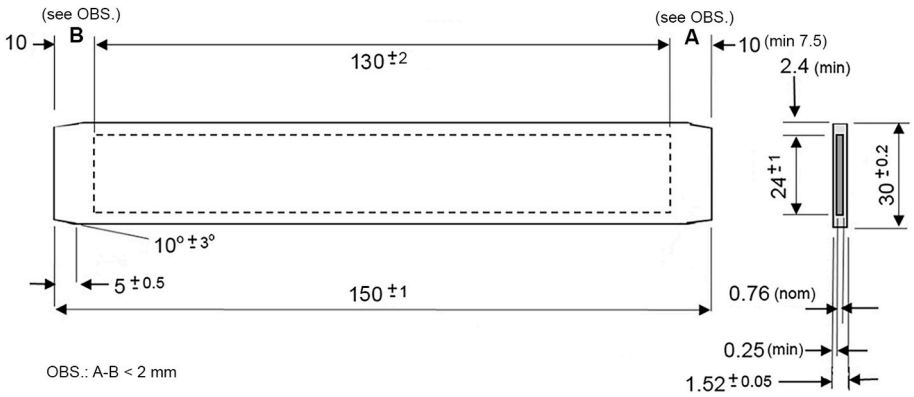

Fig. 1. Geometry of LEU target plate (all dimensions are in mm).

manufactured according to two currently available technologies. The most commercially used manufacturing technology is based on small plates containing a core (usually called "meat") comprising a U–Al compound dispersed in an aluminum matrix (Kohut et al., 2000; Ali et al., 2013; Mushtaq, 2011; Ryu et al, 2013, 2015), similar to the manufacture of fuel plates used as a nuclear fuel for research reactors. The second technology is based on thin foils of metallic uranium (Conner et al., 1999; Briyatmoko et al., 2007; Wiencek et al., 2008; Solbrekken et al., 2011).

Dispersion plate-type targets use low enriched uranium (LEU, < 20 wt% U-235) and are manufactured according to the traditional picture-frame technique adopted for the commercial production of fuel elements for nuclear research reactors. Kohut et al. (2000) developed this type of target using a mixture of UAl_2 and aluminum powders compacted to form the UAl_2–Al dispersion. UAl_2 was produced by melting uranium and aluminum together. The ingot of UAl_2 is then crushed into powder to fabricate UAl_2–Al dispersion plates according to the picture-frame technique. Ali et al. (2013) describe the primary procedures for manufacturing plate-type dispersion targets, and Mushtaq (2011) describes the qualification procedures.

Kaufman (1962) first described the picture-frame technique, and Durazzo and Riella (2015) give detailed information about this manufacturing technique. In the picture-frame technique, a core containing the uranium compound (also called "briquette") is placed in a "picture-frame" plate with a hole matching the briquette outline in the center. Two cladding plates with the same dimensions are assembled over and under the frame plate. The assembly is TIG (tungsten inert gas) welded and then is hot- and cold-rolled to the final thickness. This technique is extensively used for manufacturing plate-type fuel elements for research reactors. Aluminum is used to fabricate the frame and claddings plates. After rolling, the starting briquette forms a "meat" containing the uranium. The meat is completely surrounded by aluminum, guaranteeing the removal of the heat generated in the fission and its isolation from the reactor environment.

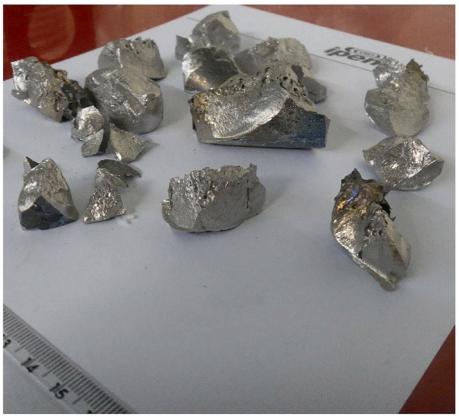

Fig. 2. Pieces of the UAl_2 ingot produced by induction melting.

The Nuclear and Energy Research Institute (IPEN/CNEN-SP) has been routinely fabricating LEU fuel elements for the IEA-R1 research reactor. To date, over 150 fuel elements have been fabricated, including the fuel elements that compose the new core of the IPEN-MB-01 critical facility (19 fuel elements). These new fuel elements meet the specifications for the RMB fuel. The fuel is plate-type using the LEU U_3Si_2–Al dispersion. Because of the experience gained over the years in manufacturing the fuel elements, it was decided to implement this technology to fabricate UAl_x-Al plate-type dispersion targets for future Mo-99 production in Brazil.

The binary uranium/aluminum system forms a phase diagram that shows intermetallic compounds comprising three phases, namely UAl_2, UAl_3, and UAl_4. The mixture of these phases is well-known in the literature as UAl_x. Among those uranium aluminides compounds, uranium dialuminide (UAl_2) has been used as a starting material to fabricate the irradiation targets. The use of UAl_2 has the advantage of having a congruent melting point which allows it to be synthesized in a single step. On the other hand, the superior aluminides (UAl_3 and UAl_4) require long thermal treatments to be synthesized since they have incongruent melting points and are formed through peritetic reactions (Okamoto, 2012). In addition, UAl_2 has higher U content (81.52 wt% U) and higher density (8.14 g/cm^3) than the other uranium aluminides, which maximizes the U-235 content in the target.

During target fabrication, according to the picture-frame technique (hot-rolling and annealing), a solid-state reaction takes place between UAl_2 and aluminum to form the higher aluminides, UAl_3 and UAl_4. Uranium aluminides have different chemical properties in terms of their dissolution in a basic medium to extract molybdenum-99 after irradiation. Cols et al. (2000) reported that UAl_3 and UAl_4 dissolve more easily in the alkaline medium than UAl_2. The efficiency of the dissolution is vital for maximizing the yield of the radiochemical processing for the extraction of Mo-99. For this reason, the UAl_2 content in the finalized target should preferably be zero. In this way, the thermomechanical treatment adopted for manufacturing the targets must guarantee that the UAl_2 is totally consumed (or reduced to the minimum) in the final target.

An innovative technique was developed at this work that allowed increasing the productivity of LEU dispersion plate-type target, which is based on rolling multiple briquettes in the same rolling operation. A single briquette is usually used in each rolling operation for target fabrication by the picture-frame technique. The manufacturing parameters of uranium aluminide dispersion targets were defined by applying the new technique. Thermomechanical processing to control the aluminide phases present in the meat of the final target was developed. The manufacturing process proved suitable for producing LEU targets fulfilling the specification to produce Mo-99 in the Brazilian Multipurpose

Table 1
Composition, density, and impurities of UAl_2 powder.

Phase Composition	UAl_2	UAl_3	UAl_4	UO	UO_2
(%)	87.1 ± 0.3	10.2 ± 0.3	N.D	1.6 ± 0.1	1.2 ± 0.1
Uranium Total (%)	80.74 ± 0.02				
Density (g/cm^3)	8.13 ± 0.01				
Element	(μg/g)	Element	(μg/g)	Element	(μg/g)
Li	<0.1	Co	<0.4	Sm	<0.4
B	<0.4	Ni	16.6 ± 0.2	Eu	<0.1
Mg	1.7 ± 0.1	Cu	9.4 ± 0.2	Gd	<0.1
Si	<3.0	Zn	2.3 ± 0.1	Dy	<0.2
Ca	4.4 ± 0.5	Mo	<3.0	Ti	0.96 ± 0.05
V	3.8 ± 0.1	Cd	<0.1	Ta	<0.1
Cr	3.1 ± 0.2	Ba	<0.2	W	<0.4
Mn	16.3 ± 0.1	Pb	<6.0		
Fe	64 ± 1	Sn	1.7 ± 0.1		

N.D = not detected.

Reactor.

2. Experimental

According to the first calculations, the LEU target plate must incorporate 1.12 g of U-235 in a meat 130 mm long and 24 mm wide. Fig. 1 shows the target's geometry.

Natural uranium in metallic form and aluminum metal was used as starting material to synthetize UAl_2. Uranium metal was produced at IPEN/CNEN-SP employing magnesiothermic reduction of UF_4 according to the procedures described by Durazzo et al. (2017). The starting materials were weighed stoichiometrically (81.5wt% U), charged into a zirconium crucible, and melted using a 15-kW induction furnace. Before the melting, the furnace was purged with argon after reaching $2.6.10^{-3}$ mbar. Fig. 2 shows a view of the produced UAl_2 ingot. The material was fragile and broke into several pieces.

Powder metallurgy techniques were used in the manufacture of the briquette. The briquette was made with powdered UAl_2 and pure aluminum powder, which was the structural matrix material of the briquette. The UAl_2 ingot was ground under an argon atmosphere (the material is pyrophoric) using a hand mill and sieved to separate the sizes: > 88 μm, 88 μm–44 μm, and <44 μm. The UAl_2 powder had the composition of 80 wt% 88 μm–44 μm and 20 wt% <44 μm. The density of the UAl_2 powder was 8.13 ± 0.01 g/cm^3, determined in triplicate by helium pycnometry. The uranium content was 80.74 ± 0.02%, determined in triplicate using the Davis-Gray method (Davies and Gray, 1964; Bickel, 1997).

The phase composition was quantified by X-ray diffraction according to a method developed in prior studies (Conturbia et al., 2018). X-ray diffraction data were collected using a Bruker diffractometer, operating with Cu-Kα radiation at 40 kV and 30 mA, with a scan of 0.02° and 8-s counts per step. Table 1 summarizes all chemical and physical analyzes carried out on the UAl_2 powder.

The powders for each individual briquette were separately weighed and combined for blending. The composition of the mixtures was 45 vol % of UAl_2 powder and 50 vol% of aluminum powder (99 % purity). The mixtures were homogenized for 1 h in a Turbula T2F mixer and compacted under a pressure of 460 MPa to produce briquettes with residual porosity of around 5 vol%. The briquettes were compacted at room temperature using a floating die lubricated with stearic acid. The briquette was a straight prism with a square base (22 × 22 mm) with

Table 2
Main typical characteristics of briquettes.

Dimensions (mm)	22.16 X 22.15 X 4.20 (thickness) (with rounded corners/R = 3.0 mm)	
Briquette	Mass (g)	9.67
	Volume (cm^3)	1.94
UAl_2	Mass (g)[a]	7.02
	Volume (cm^3)	0.86
	Volume fraction (%)	44.4
Aluminum	Mass (g)	2.65
	Volume (cm^3)	0.98
	Volume fraction (%)	50.3
Pores	Volume (cm^3)	0.10
	Volume fraction (%)	5.2

[a] Equivalent to 1.12 g U-235 (enrichment 19.75 wt%).

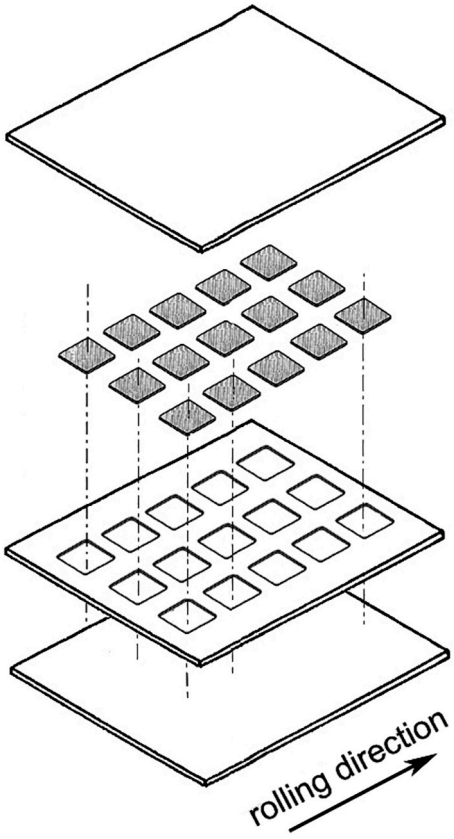

Fig. 3. Assembling the briquettes/frame/covers for rolling.

rounded corners and a height of 4.2 mm.

The briquettes were degassed at 250 °C for 3 h under vacuum (5.10^{-3} Pa). The mass of UAl_2 was calculated to incorporate the equivalent of 1.12 g of U-235 into the target meat. Table 2 presents the typical characteristics of briquettes.

The briquettes were assembled into a 6061-aluminum picture-frame (4.20 mm thick) containing 15 cavities and cladded with two 6061-aluminum cover plates (2.86 mm thick), as shown in the scheme at Fig. 3.

The assembly was TIG (Tungsten Inert Gas) welded together and then rolled to form the targets. The briquettes and frame were bonded to the covers by hot bonding during hot-rolling processing. The assembly was hot-rolled in six rolling passes. After rolling, the briquettes form the "meats" of the targets. The assembly is converted into plate to provide the required dimensions and complete sealing of the meats. The frame provides both lateral support for the briquettes and material for bonding with the cover plates. The final thickness for the target was reached

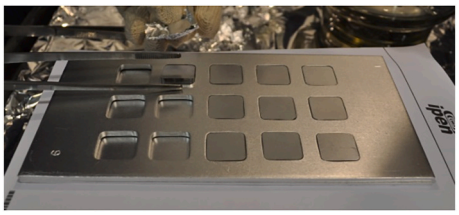

Fig. 4. Illustration of the assembling operation.

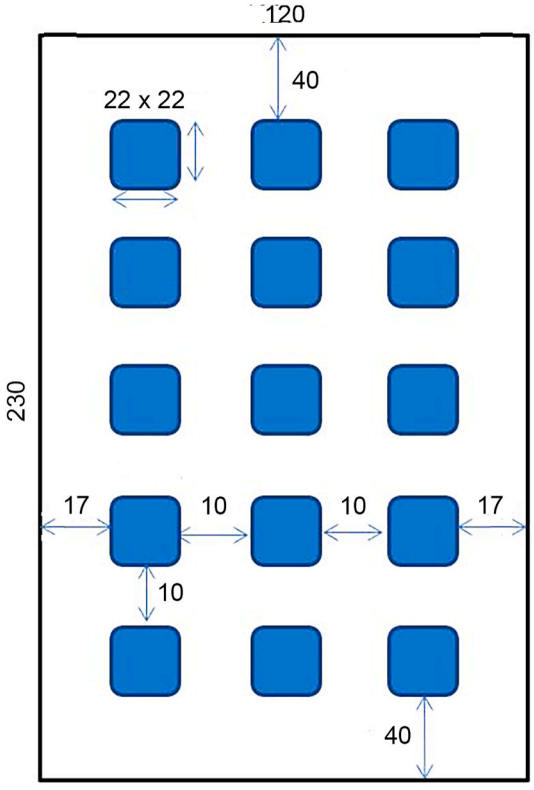

Fig. 5. Illustrative diagram of the frame plate containing multiple cavities (dimensions in mm).

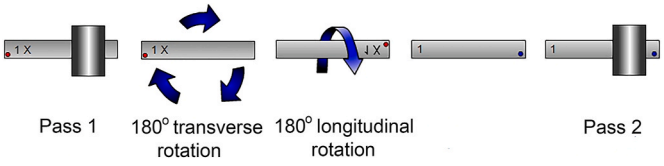

Fig. 6. Rotation scheme of the assembly in hot-rolling.

through cold-rolling. The rolling scheme was defined based on previous work (Conturbia et al., 2018).

All briquettes were rolled simultaneously. Thus, in the same rolling operation, a plate (called "mother plate") containing 15 targets was produced. The cavities in the frame plate were manufactured with a gap of 0.2 mm to allow easy assembly of the briquettes in each cavity. Fig. 4 illustrates the assembling of the briquettes. Fig. 5 presents details of the frame plate.

The rolling temperature was 540 °C, and the reheating time between rolling passes was 36 min. Before the first rolling pass, the assembly was preheated for 1 h. The assembly was rotated about their longitudinal and transverse axis between passes to control the end defects and cambering, as shown in Fig. 6. The leading end defects are dog-boning and "diffuse zone". Inevitably, the rolling process leaves the ends of the meat thicker than the middle. The longitudinal cross-section of fuel meat with thickened ends resembles a bone, hence the name. The "diffuse zone" refers to the defects known as "fish-tail". Durazzo and Riella (2015) describe the end defects. After the last hot-rolling pass, the plate was kept for 3 h at 540 °C. The total heating time was 420 min (7 h). Table 3 presents the rolling schedule used to fabricate the "mother plate".

After the thermal treatment, the plate was removed from the furnace, allowed to air-cool, and examined for blister formation. Both sides of the plate were visually inspected under an incident light to detect blisters. If there is a lack of metallurgical bonding, enclosed air in the non-bonded area will inflate and create a blister at the plate's surface. A blister larger than 1.5 mm in diameter directly over the fuel zone or 3 mm in diameter at the non-fuel zone indicates poor bonding and is a cause of rejection.

After cold rolling, the "mother plate" was cut at its ends (pre-cut) and straightened using a roll leveler. No reduction in thickness was accomplished during the straightening operation. A hydraulic guillotine was used to make all the cuts.

The metallurgical bonding was inspected using extensive bending tests carried out on the ends trimmed off the "mother plate" in the pre-cut. Bend test samples were taken from all four sides of the "mother plate". Each sample was clamped in a test fixture and bent around a mandrel 90° in one direction, returned to 0°, bent 90° in the opposite direction, and returned to 0°. The edges of the sample were then visually examined for delamination. Any strip showing delamination of the cladding layers is determined to be unbonded, and the associated plate is rejected. Six bend samples from the "mother plate" were tested, two from each length side and one from each width side.

After the pre-cut, the "mother plate" was then radiographed to locate the individual targets. Fig. 7 shows the digital radiography.

Through the digital radiography shown in Fig. 7, four cuts were made to separate 5 pieces of the "mother plate" containing three targets each. The piece was radiographed again, and lines were digitally drawn based on the radiographic image. The lines were defined based on the dimensional specification of the target shown in Fig. 1. The drawn lines were mechanically transferred to the piece employing a sharp steel scriber. The lines outline the individual targets and will guide the final cut. Fig. 8 illustrates a radiographic image of a piece where all lines were delineated according to the target's specification. Based on the drawn lines, the final cut was made. In this way, all targets were extracted from the "mother plate".

All the external dimensions of each individual target were inspected using either caliper for length inspection or a micrometer for width inspection. The caliper and micrometer precisions used in these measurements were 0.02 mm and 0.01 mm, respectively. The thicknesses were also inspected with a micrometer with nonrotating spindles having chamfered edges.

Before the final cut, another radiograph (defect radiograph) is performed on the pieces removed from the "mother plate" to check the meats for defects and uranium homogeneity. Fig. 9 shows a typical radiograph to evaluate the homogeneity. A final radiograph is done to inspect the internal positioning of the meat.

A destructive test was performed to measure the thicknesses of the meat and claddings on the finished target. This inspection is one of the most critical controls that must be carried out. The cladding thickness of the target is of great importance; therefore, it is strictly specified. The inspection comprises taking four samples from the target and measuring claddings and meat thickness using metallography. Two samples were taken from each end of the meat, and two are taken from the center (one longitudinal and one transversal to the rolling direction), as shown in Fig. 10. The measurement was performed by taking the minimum values of the claddings in each sample in selected positions where visually the cladding thickness is decreased. Five targets were inspected by metallography, taken from different regions of the "mother plate". Fig. 11 shows the positions on the "mother plate" from which the targets were withdrawn.

Table 3
Thermomechanical treatment for manufacturing the targets into the "mother plate".

	Pass	Designed		Actual		
	Number	thickness (mm)	reduction (%)	thickness (mm)	reduction (%)	time at 540 °C (min)
pre-heating						60
	start	9.92				
	1	6.94	30	7.04	29.0	36
	2	5.21	25	5.20	26.1	36
hot	3	3.91	25	3.95	24.0	36
	5	2.93	25	2.90	26.5	36
	6	2.20	25	2.21	23.7	36
	end	1.69	23	1.70	23.1	
thermal treatment (blister test)						180
					total	420 (7 h)
cold	1	1.61	5	1.60	5.9	
	2	1.52	5	1.53	4.4	

Fig. 7. Digital radiography of the "mother plate" showing the individual targets.

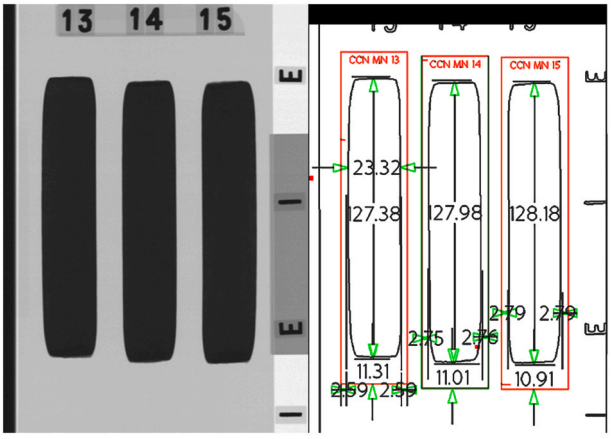

Fig. 8. At left, a Digital X-ray image of the targets. At right, an example of the delineation process.

For metallographic inspection, the samples were adequately identified and were embedded in acrylic resin. Once the samples were embedded, each sample was prepared according to the following steps: grinding with SiC 320 grit-paper; grinding with SiC 600 grit-paper; grinding with SiC 1200 grit-paper; polishing with 6 μm diamond paste; polishing with 3 μm diamond paste; and final polishing with 0.02 μm colloidal silica slurry.

For each step, a grinding time of 3 min was used (70 rpm). For the steps of diamond polishing, a polishing time of 15 min was used (70 rpm). For the final polishing step, a polishing time of 5 min was used.

The thickness of the claddings and meat were measured in the cross sections of the polished samples using a Zeiss optical microscope, model Axio Imager M2m coupled to an image analyzer.

The content of aluminides phases present in the finished target was measured in 3 targets according to the method described by Conturbia et al. (2018).

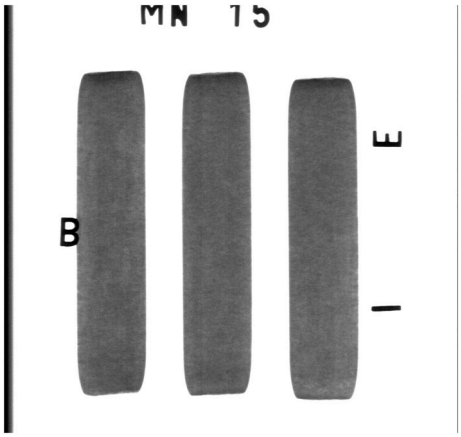

Fig. 9. Typical radiograph to evaluate defects and distribution of uranium in the meat. This image shows a good homogeneity between UAl_x and Al.

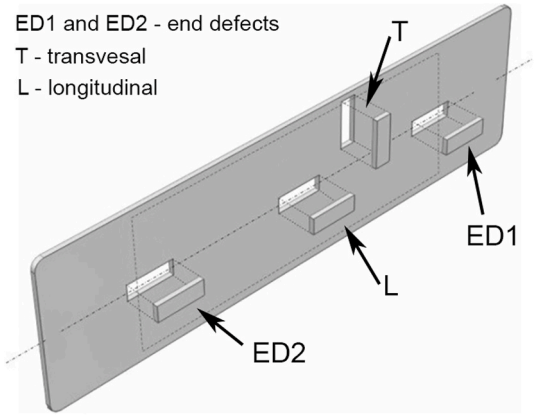

Fig. 10. Samples of the target that were evaluated for claddings and meat thicknesses.

3. Results and discussion

Cols et al. (2000) reported that UAl_3 and UAl_4 are more easily dissolved in alkaline solutions than UAl_2. However, UAl_2 has higher uranium content than UAl_3 and UAl_4, which maximizes the U-235 content in the target. Besides, UAl_2 has congruent solidification (easy to produce) and is fragile (easily ground to a powder). These are the reasons that make it interesting for use as starting material in the manufacture of

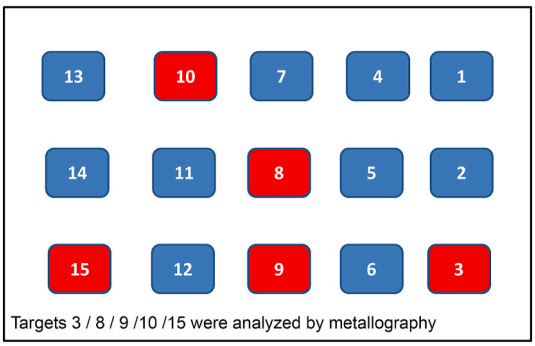

Fig. 11. Targets selected for metallographic inspection.

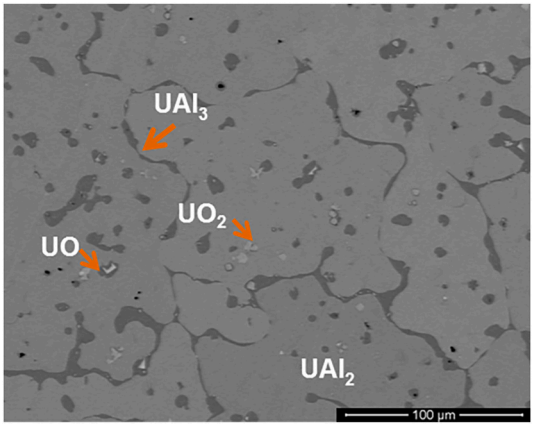

Fig. 12. Scanning electron microscope (SEM) image of primary UAl_2 ingot (backscattered electrons). Four phases can be seen.

targets. A scanning electron micrograph of the primary UAl_2 ingot produced in this work is shown in Fig. 12. Because of the atomic number contrast obtained from backscattered electrons, which is sensitive to the composition, it was possible to observe four shades of gray, indicating four phases.

Fig. 12 shows the formation of UAl_2 as the predominant phase, which is shown in a lighter gray tone. UAl_3 appears as the minority phase, which was formed during the solidification of the residual liquid phase in the grain boundaries of UAl_2. This phase is shown in a darker gray tone in Fig. 12. Inclusions in shades of gray even lighter than UAl_2 can be seen in the image. Because of the microscopy method used (backscattering), it can be inferred that these inclusions come from denser phases than UAl_2. X-ray dispersive energy spectra (EDS) were collected from each region separately, as shown in Fig. 13. Semi-quantitative analyzes from the regions assigned to UAl_2 and UAl_3 confirm the image obtained with backscattered electrons. The inclusion in a lighter gray tone than UAl_2 showed a composition close to UO_2.

The almost white phase was identified as UO and was mainly embedded in the UAl_3 phase. The phase slightly less dense than UAl_2 (light gray than UAl_2) was identified as UO_2 and was embedded in the UAl_2 matrix. The composition of the phases was determined by X-ray Diffraction. The results are presented in Table 4.

The preparation of a pure intermetallic depends on the experimental conditions of the atmosphere during the melting process, the purity of the raw materials, and the method used for synthesis. From a productive point of view, there will always be a residual amount of compounds on the left and right sides in the phase diagram around the desired composition, as reported in the literature by Wiencek (1995) for the U–Si system and also by Ali et al. (2013) for the U–Al system. The presence of UAl_3 – left side of the Al–U diagram reported by Okamoto (2012) – was observed in our work. However, from a practical and productive point of view, UAl_3 does not cause technical difficulties in manufacturing targets since it will be formed in the solid-solid reaction UAl_2–Al during the manufacture. The presence of UAl_3, because of its ductile character, could make it difficult to grind the UAl_2 ingot for the production of powder. However, the UAl_3 present at the level existing in our UAl_2 ingot did not cause any grinding difficulty. The ingot was easily powdered.

Small quantities of oxides are inevitable when preparing UAl_2. Ali

Table 4
Phase composition in primary UAl_2 ingot.

UAl_2 wt%	UAl_3 wt%	UAl_4 wt%	UO wt%	UO_2 wt%
87.1 ± 0.3	10.2 ± 0.3	N.D	1.6 ± 0.1	1.2 ± 0.1

N.D = not detected.

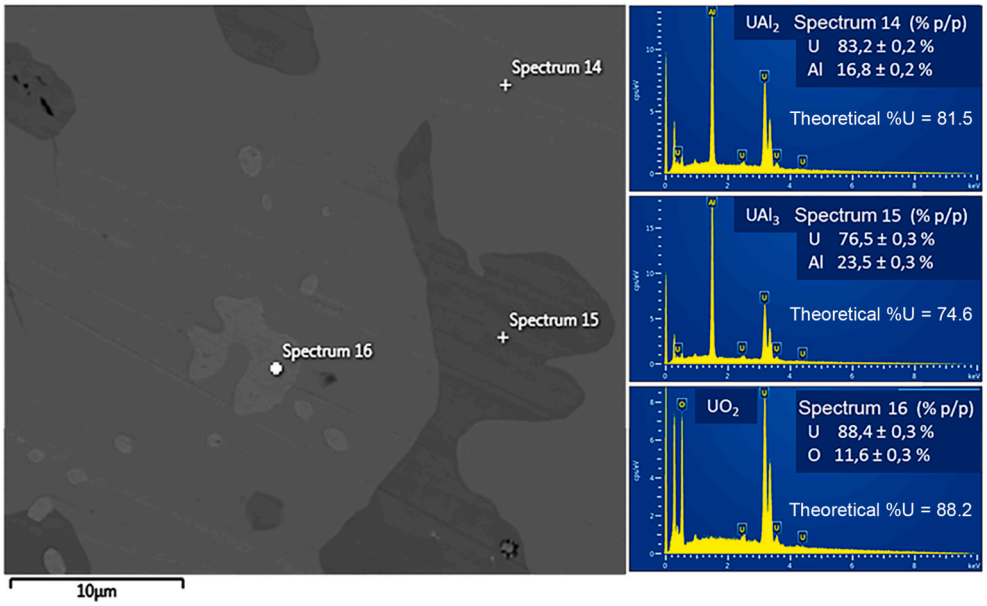

Fig. 13. Backscattered electron image of the ingot with the respective regions where the EDS spectra were collected.

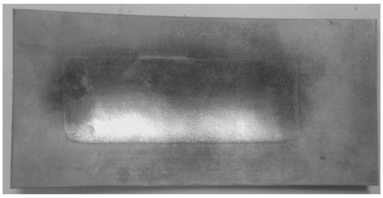

Fig. 14. Increase target meat volume because of the transformation of UAl_2 into UAl_3 and UAl_4 (after heat treatment at 540 °C for 9 h).

Table 5
Phase composition in the finished target.

UAl_2 wt%	UAl_3 wt%	UAl_4 wt%	UO wt%	UO_2 wt%
0.3 ± 0.1	30.1 ± 1.5	68.1 ± 1.6	0.3 ± 0.1	1.3 ± 0.2

N.D = not detected.

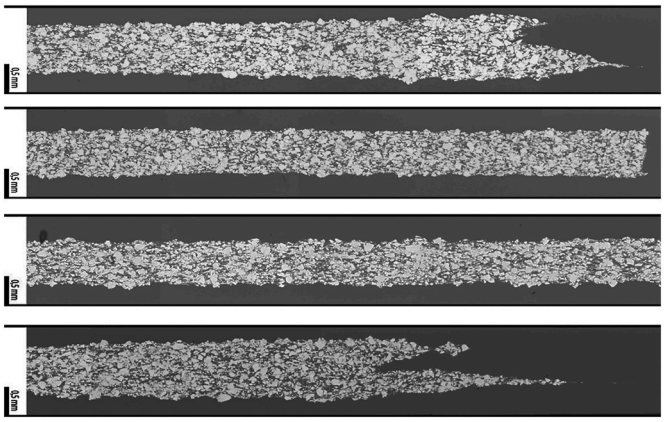

Fig. 15. Cross-section views of the target observed in SEM (backscattered electrons). Top: end defect region 1. Top middle: transversal region. Bottom middle: longitudinal region. Bottom: end defect region 2. (see Fig. 10).

et al. (2013) detected oxides in concentrations between 2 and 4.7 wt% in their UAl_2 samples synthetized by arc melting. These authors did not discriminate the composition of the oxides, and they identified them as UO/UO_2. Kohut et al. (2000) also detected UO_2 peaks in the diffractogram obtained from their UAl_2 samples made by induction melting. Oxides are difficult to avoid because of the high reactivity of the uranium metal used as raw material. Small amounts of oxygen present as a contaminant in the furnace atmosphere cause oxidation.

The reaction of UAl_2 with the aluminum matrix of the dispersion, transforming into UAl_3/UAl_4, results in an increase in volume because of the lower densities of aluminum-rich aluminides. According to Matos and Snelgrove (1992), the density of UAl_2 is 8.1 g/cm^3, that of UAl_3 is 6.8 g/cm^3, and that of UAl_4 is 6.1 g/cm^3. A high-volume increase was observed in the samples after heat treatment at 540 °C for 9 h, as shown in Fig. 14. Assuming the composition of 10 wt% UAl_3 and 90 wt% UAl_4 after the heat treatment, the volume increase was estimated to be around 25 % (Conturbia et al., 2018). This exaggerated swelling is undesirable in cold-rolling, which can cause damage to the surface of the target at the end of the meat, such as cracks and marks, as well as problems of dog-boning and fish-tail end defects (Durazzo and Riella, 2015). For this reason, the UAl_2 transformation into UAl_3 and UAl_4 should be distributed along the hot-rolling process so that part of the volume increase because the reaction is gradually absorbed during the hot-rolling.

In this work (see Table 5), the target contained virtually no residual UAl_2 at the end of manufacture. The thermomechanical treatment used

Table 6
Thicknesses of claddings and meats of selected samples as shown in Figs. 10 and 11.

Specification		≥0.25 (mm)	≤1.07 (mm)	≥0.25 (mm)
		cladding 1	meat	cladding 2
target 3	ED1	0.30	0.91	0.32
		0.37	0.80	0.36
	T	0.36	0.81	0.36
		0.38	0.77	0.38
		0.35	0.85	0.33
	L	0.37	0.81	0.35
		0.36	0.83	0.34
	ED2	0.27	0.95	0.31
target 8	ED1	0.33	0.89	0.31
		0.35	0.83	0.36
	T	0.36	0.83	0.35
		0.37	0.80	0.35
		0.35	0.83	0.36
	L	0.36	0.81	0.36
		0.34	0.85	0.35
	ED2	0.33	0.87	0.33
target 9	ED1	0.26	0.95	0.33
		0.36	0.80	0.38
	T	0.38	0.80	0.36
		0.35	0.83	0.36
		0.34	0.85	0.34
	L	0.38	0.80	0.36
		0.34	0.82	0.37
	ED2	0.27	0.95	0.31
target 10	ED1	0.32	0.88	0.34
		0.35	0.85	0.34
	T	0.36	0.82	0.36
		0.36	0.81	0.37
		0.36	0.82	0.36
	L	0.36	0.83	0.35
		0.37	0.80	0.37
	ED2	0.33	0.85	0.36
target 15	ED1	0.26	0.97	0.29
		0.36	0.83	0.33
	T	0.34	0.83	0.36
		0.35	0.82	0.35
		0.34	0.84	0.35
	L	0.36	0.82	0.35
		0.35	0.82	0.35
	ED2	0.27	0.97	0.28

resulted in the transformation of nearly all UAl_2 initially present, which was distributed throughout the entire manufacturing process. In this way, most of the swelling because of the transformation was absorbed slowly during hot-rolling, and the end defects could be efficiently controlled. Fig. 15 shows the typical microstructure of the central region end defects observed in the targets.

The cladding and meat thicknesses measured by metallography in the samples (see Fig. 10) extracted from five targets manufactured in different regions of the "mother plate" (see Fig. 11) are shown in Table 6. All claddings (of all targets) have higher thicknesses than 0.25 mm, meeting the specification. An example of cladding thickness measurement is presented in Fig. 16. The figure shows optical images got at the end defects region (sample ED2 and ED1 from the target 9).

The inspections of metallurgical bonding and homogeneity in the meat of the targets gave identical results to those observed in the routine manufacturing of fuel plates. Neither blister was detected by visual inspection, nor bonding failures were detected in the bending tests. The homogeneity of the uranium distribution in the meat of all targets was satisfactory. Also, the "mother plate" behavior during manufacture was very similar to that observed in the manufacture of traditional fuel plates.

The distribution of the 15 targets on the "mother plate" (Fig. 7) after rolling proved to be controllable, allowing cutting individual meats without significant difficulties. The delineation method for the

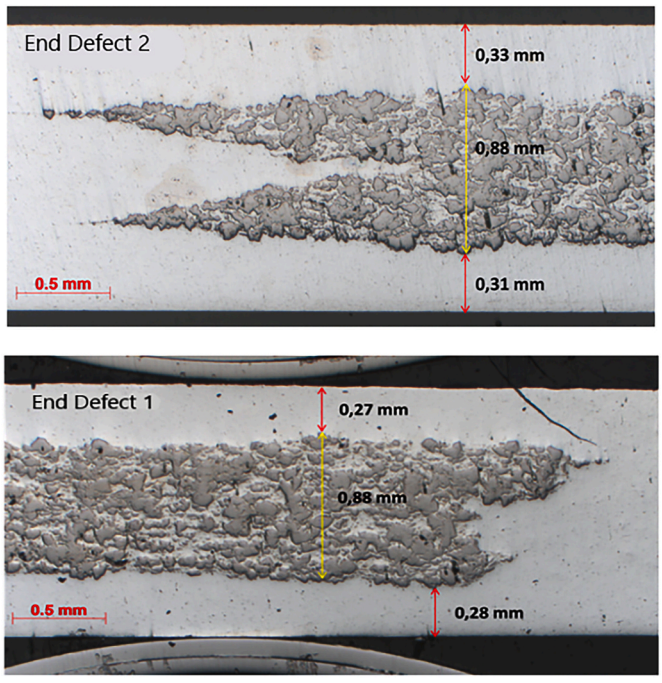

Fig. 16. Example of cladding thickness measurement by optical microscopy from the target 9.

Table 7
Dimensions of the meats and thicknesses of finished targets.

	meat width (mm)	meat length (mm)	target thickness (mm)
target 1	24.49	130.88	1.53
target 2	24.36	131.33	1.53
target 3	24.43	130.47	1.53
target 4	24.32	130.33	1.54
target 5	24.27	129.83	1.54
target 6	24.32	130.30	1.54
target 7	24.31	130.50	1.53
target 8	24.27	130.53	1.53
target 9	24.33	130.53	1.53
target 10	24.28	130.34	1.54
target 11	24.30	130.50	1.54
target 12	24.31	130.17	1.53
target 13	24.42	131.28	1.54
target 14	24.40	130.68	1.54
target 15	24.45	130.50	1.53

orientation of the final cut proved to be efficient. The dimensions of the meats of all targets have met the specification. This result demonstrates that the individual deformation of the targets was homogeneous regardless of their position on the "mother plate". Table 7 presents these results.

4. Conclusions

Manufacturing multiple targets from a single "mother plate" has been carried out successfully. The results showed that fifteen targets can be manufactured simultaneously in a single rolling operation. The concept of "mother plate" showed that it is possible to achieve a significant increase in the productivity of targets, consequently reducing the cost of production. The maximum number of targets that can be incorporated on the "mother plate" depends only on the geometry of the initial briquettes and the frame plate. The LEU UAl_2 used as raw material was successfully manufactured using induction melting. The manufacturing and qualifying procedures are similar to the ones used to produce traditional fuel plates. A thermomechanical treatment was designed to get targets composed basically of a mixture of UAl_3/UAl_4 that are the required phases for a proper radiochemical dissolution after irradiation. All fabrication parameters were defined, and the specifications have been fulfilled. The manufacturing procedures are suitable considering a domestic scenario where the targets will be fabricated at the Brazilian Nuclear Fuel Center and used at the Brazilian Multipurpose Reactor (RMB). Futures studies and developments are in progress, aiming to design targets with higher U-235 load.

Declaration of competing interest

The authors declare that they have no known competing financial interests or personal relationships that could have appeared to influence the work reported in this paper.

Acknowledgments

The authors are grateful to CNPq (National Council for Scientific and Technological Development) for the research grants 454147/2017-1, 304034/2015-0, and 471008/2011-7 provided for this work. The authors would also like to thank São Paulo Research Foundation (FAPESP) for the research grants 2011/13849-9 and 2018/18228-1. The Brazilian Nuclear Fuel Center technicians are acknowledged for their careful hands-on work during all steps of the fabrication and characterization.

References

Ali, K.L., Khan, A.A., Mushtaq, A., Imtiaz, F., Zial, M.A., Gulzar, A., Farooq, M., Hussain, N., Ahmed, N., Pervez, S., Zaidi, J.H., 2013. Development of low enriched uranium target plates by thermo-mechanical processing of UAl_2-Al matrix for production of 99Mo in Pakistan. Nucl. Eng. Des. 255, 77–85. https://doi.org/10.1016/j.nucengdes.2012.10.014, 2013.

Barnowski, R., 2011. Insourcing nuclear medicine, 2011 J. Sci. Pol. Govern. 1, 1–4. available at: https://www.sciencepolicyjournal.org/uploads/5/4/3/4/5434385/_insourcing_nuclear_medicine.pdf.

Bickel, M., 1997. The Davies-Gray titration for the assay of uranium in nuclear materials: a performance study. J. Nucl. Mater. 246, 30–36. https://doi.org/10.1016/S0022-3115(97)00040-8, 1997.

Briyatmoko, B., Guswardani, B., Purwanta, S., Permana, S., Basiran, D., Kartaman, M., 2007. Indonesia's current status for conversion of Mo-99 production to LEU fission. In: Proceeding of International Meeting on Reduced Enrichment for Research and Test Reactors, Prague, Czech Republic, pp. 23–27. September, 2007 (available at: Indonesia's Current Status for Conversion of Mo-99 production to LEU Fission (anl.gov).

Cols, H.J., Cristini, P.R., C Manzini, A., 2000. Mo-99 from low-enriched uranium. In: Proceeding of International Meeting on Reduced Enrichment for Research and Test Reactors, Las Vegas, Nevada, 1-6 October, 2000 available at: http://www.rertr.anl.gov/Web2000/Title-Name-Abstract/Cristi00.html.

Conner, C., Lewandowsk, I.E.F., Snelgrove, J.L., Liberatore, M.W., Walker, D.E., Wiencek, T.C., Mcgann, D.J., Hofman, G.l., Vandergrift, G.F., 1999. Development of annular targets for 99Mo production. In: Proceeding of International Meeting on Reduced Enrichment for Research and Test Reactors, Budapest, Hungary, 3-8 October, 1999 available at: DEVELOPMENT OF ANNULAR TARGETS FOR 99MO PRODUCTION (anl.gov).

Conturbia, G.L.C.R., Durazzo, M., Urano de Carvalho, E.F., Riella, H.G., 2018. Phase quantification in UAl_x-Al dispersion targets for Mo-99 production. J. Nucl. Mater. 509, 465–477. https://doi.org/10.1016/j.jnucmat.2018.07.029, 2018.

Davies, W., Gray, W., 1964. A rapid and specific titrimetric method for the precise determination of uranium using iron(II) sulphate as reductant. Talanta 11 (8), 1203–1211. https://doi.org/10.1016/0039-9140(64)80171-5, 1964.

Durazzo, M., Riella, H.G., 2015. Procedures for Manufacturing Nuclear Research Reactor Fuel Elements. OmniScriptum GmbH & Co. KG, Saarbrücken, Germany, 2015.

Durazzo, M., Saliba-Silva, A.M., Martins, I.C., Urano de Carvalho, E.F., Riella, H.G., 2017. Manufacturing low enriched uranium metal by magnesiothermic reduction of UF_4. Ann. Nucl. Energy 110, 874–885. https://doi.org/10.1016/j.anucene.2017.07.033, 2017.

Kaufman, A.R., 1962. Nuclear Reactor Fuel Elements, Metallurgy and Fabrication. Interscience, New York, N.Y, 1962.

Kohut, C., Fuente, M., Echenique, P., Podesta, D., Adelfang, P., 2000. Targets development of low enrichment for production of Mo99 for fission. In: Proceeding of International Meeting on Reduced Enrichment for Research and Test Reactors, Las Vegas, Nevada, 1-6 October, 2000 available at: https://www.rertr.anl.gov/Web2000/Title-Name-Abstract/Fuente00.html.

Matos, J.E., Snelgrove, J.L., 1992. Fuels (Appendice I-1.1). Research Reactor Core Conversion Guidebook, vol. 4. International Atomic Energy Agency, Vienna, 1992. IAEA-TECDOC-643 (available at: te_643v4_prn.pdf (iaea.org).

Mushtaq, A., 2011. Specifications and qualification of uranium/aluminum alloy plate target for the production of fission molybdenum-99. Nucl. Eng. Des. 241, 163–167. https://doi.org/10.1016/j.nucengdes.2010.11.003, 2011.

Nuclear Energy Agency, 2019. The Supply of Medical Radioisotopes: 2019 Medical Isotope Demand and Capacity Projection for the 2019-2024 Period. OECD Publishing, Paris, 2019. NEA/SEN/HLGMR(2019)1 (available at: https://www.oecd-nea.org/med-radio/docs/sen-hlgmr2019-1.pdf.

Obadia, I.J., Perrotta, J.A., 2010. A sustainability analysis of the Brazilian Multipurpose reactor project. In: International Topical Meeting on Research Reactor Fuel Management RRFM 2010, Marrakech, Morocco, 21-25 March, 2010 available at: https://www.euronuclear.org/download/proceedings-rrfm-2010/?wpdmdl=3046&refresh=5fecaed7e2c961609346775.

Okamoto, H., 2012. Al-U (Aluminum-Uranium). J. Phase Equilibria Diffus. 33 (6), 489–490. https://doi.org/10.1007/s11669-012-0089-x, 2012.

Perrotta, J.A., Obadia, I.J., 2011. The RMB Project development status. In: Proceeding of International Conference on Research Reactors: Safe Management and Effective Utilization. Session C: New Research Reactor Projects. 14-18 November 2011, Rabat, Morocco. Proceeding series. International Atomic Energy Agency, 2012. (available at: https://www-pub.iaea.org/MTCD/Publications/PDF/P1575_CD_web/datasets/abstracts/C6Perrotta.html.

Perrotta, J.A., Soares, A.J., 2014. RMB: the new Brazilian Multipurpose research reactor. In: International Topical Meeting on Research Reactor Fuel Management RRFM 2014, Ljubljana, Slovenia, 20 March-3 April, pp. 394–401, 2014 (available at: https://www.euronuclear.org/download/proceedings-rrfm-2014/.

Ryu, H.J., Kim, C.K., Sim, M.S., Park, J.M., Lee, J.H., 2013. Development of high-density U/Al dispersion plates for Mo-99 production using atomized uranium powder. Nucl. Eng. Technol. 45, 979–986. https://doi.org/10.5516/NET.07.2013.014, 2013.

Ryu, H.J., Jeong, Y.J., Nam, J.M., Park, J.M., 2015. Metallurgical considerations for the fabrication of low-enriched uranium dispersion targets with a high density for 99Mo production. J. Radioanal. Nucl. Chem. 305, 31–39. https://doi.org/10.1007/s10967-014-3838-y, 2015.

Solbrekken, G.L., Turner, K., Govindarajan, S., Macarewicz, P., Allen, C., 2011. Development, qualification, and manufacturing of LEU-foil targetry for the production of Mo-99. In: International Topical Meeting on Research Reactor Fuel Management RRFM 2011, Rome, Italy, 20-24 March, pp. 233–237, 2011 (available at: RRFM 2011 - ENS (euronuclear.org).

Verbeek, P., 2008. Report on Molybdenum 99 Production for Nuclear Medicine 2010-2020, Association of Imaging Producers & Equipment Suppliers november 2008 (available at: https://www.oecd-nea.org/med-radio/docs/200902_AIPESMolySupplyReport.pdf.

Wiencek, T.C., 1995. Summary Report on Fuel Development and Miniplate Fabrication for the RERTR Program 1978 to 1990. Argonne National Laboratory, Argonne, Illinois, 1995. ANL/RERTR/TM-15. (available at: https://www.osti.gov/servlets/purl/125105.

Wiencek, T.C., Vandergrift, G.F., Bakel, A., Leyva, A.A., Hebden, A.S., 2008. Status and progress of foil and target fabrication activities for the production of 99Mo from LEU. In: In: Proceeding of International Meeting on Reduced Enrichment for Research and Test Reactors, Washington, DC, 5-9 October, 2008 available at: Microsoft Word - S15-P4 Wiencek-Vandegrift-Bakel-Leyva-Hebden Status and Progress of Foil and Target Fabrication Activities for (anl.gov).